JJMIE

Volume 19, Number 1, March. 2025
ISSN 1995-6665
Pages 13– 26
https://doi.org/10.59038/jjmie/190102
Editor-in-Chief: Prof. Ali M. Jawarneh

Jordan Journal of Mechanical and Industrial Engineering

Investigation of Heat Transfer and Swirl Flow Between Concentric Cylinders

Mohanad Abdulkhudhur Jasim[1], Yaser Alaiwi[2], Zainab Al-Khafaji[3,4*]

[1] Department of Mechanical Engineering, Altinbas University, Istanbul 34217, Turkey.
[2] Department of Mechanical Engineering, Altinbas University, Istanbul 34217, Turkey.
[3] Department of Civil Engineering, Faculty of Engineering and Built Environment, Universiti Kebangsaan Malaysia, 43600 UKM Bangi, Selangor, Malaysia.
[4] Department of Cooling and Air Conditioning Engineering, Imam Ja'afar Al-Sadiq University, Baghdad 10001, Iraq

Received 17 Jun 2024 Accepted 25 Nov 2024

Abstract

Swirl flows, especially in decaying forms, have shown promise in enhancing thermal performance with minimal mechanical complexity, providing a practical alternative to traditional forced convection methods in annular geometries. The swirling flows are created by introducing tangential air inflow, which promotes mixing and disrupts thermal boundary layers, thereby increasing heat transfer. This approach is valuable in applications where efficient thermal management is critical, such as in heat exchangers, reactors, and rotating machinery. This study highlights the potential effectiveness of swirling decaying flows in enhancing heat transfer, as initially proposed by Talbot. Local Nusselt numbers were experimentally measured in an annular space between concentric cylinders under a constant heat flux boundary condition. Swirling air motion was generated by tangential inlet slots, allowing air to enter with varying slot numbers and tangency angles. The resulting flow field within the annulus maintained a Reynolds number below 2000, aligning with the study's focus on low-Reynolds, laminar flow conditions for examining the impact of swirl flow on heat transfer between concentric cylinders. Careful consideration was given to keeping track of errors from their collection of sources and their propagation in the results. In heat transfer enhancement, swirling flow showed real promise; augmentation of up to 24 % could be achieved, while in power consumption, swirling flow was considerably more demanding than the fully developed non-working laminar flow. Even with the acceptable accuracy of the experimental measurements, the data reduction yielded substantial errors - up to 300 % of the calculated value - thereby undermining the results and the assumptions.

© 2025 Jordan Journal of Mechanical and Industrial Engineering. All rights reserved

Keywords: Swirling Flow; Heat Transfer Enhancement; Uncertainty Analysis.

1. Introduction

Taylor-Couette flow, defined as the fluid motion within a concentric annular gap driven by the rotation of the inner cylinder, has long been a cornerstone of research in fluid dynamics[1], [2], [3]. More recently, Taylor-Couette flow has gained renewed attention due to its complex behavior under various conditions, providing valuable insights into fundamental physics and practical applications[4], [5], [6]. Recent studies have explored the behavior of turbulent emulsions in Taylor-Couette flow, shedding light on how different fluid phases interact under rotation [7]. Furthermore, advances have been made in understanding the ultimate turbulent state of Taylor-Couette flow, characterized by asymptotic scaling for turbulent transport of both heat and angular momentum. Another critical development involves the interaction between elasticity and inertia in viscoelastic Taylor-Couette flow, a field that is providing new insights into non-Newtonian fluid behaviors. Beyond its fundamental importance, Taylor-Couette flow has numerous industrial applications, including its use in turbomachinery, rotating heat pipes, and electric motors, where understanding flow stability and heat transfer is essential for optimizing performance and prolonging equipment life[8], [9], [10], [11], [12], [13]. Managing the heat generated by the rotor in high-speed motors is crucial for preventing damage and extending service life.[14], [15] Moreover, the Taylor-Couette-Poiseuille flow, which occurs when an axial flow is superimposed on the Taylor-Couette flow, further enhances the complexity of this flow system and its practical implications [16], [17].

Forced convection in an annulus between two horizontal concentric cylinders has various technical and practical applications, including heat exchangers [18], [19], [20], [21]; therefore, much study has been done [22], [23], [24]. Small, low-cost, and efficient heat exchangers transporting more heat from their surfaces are major heat transfer subjects. Swirl flows are present in tornadoes,

* Corresponding author e-mail: p123005@siswa.ukm.edu.my.

cyclone separators, agricultural spraying equipment, heat exchangers, gasoline and diesel engines, gas turbines, and other heating devices [25], [26], [27]. The swirl flow device passively increases heat transfer by rotating bulk flow around an axis parallel to the flow direction [28]. Decaying swirl flow is a potential mass and heat transport mechanism. The fluid's spinning is applied upstream and subsequently reduced throughout the tube [29]. Swirl accelerates fluid flow angularly, shortens free area, and increases flow path [30]. Flow swirls may be generated using many methods [31], [32], [33]. One method uses a vortex generator to inject material tangentially, enabling fluid to enter axially. Different swirl intensities may be achieved by changing the axial and tangential intake fluid flow rates.

Recent investigations show that latent techniques, radically contorted tape, and wire curl embeds are smart heat move expansion tools [34]. Due to a coneliketurbulator in turbulent stream circumstances, others accomplished much of the early work on funnel-shaped ring turbulators on severe intensity move, pressure decrease, and stream-initiated vibrations [35]. Another study examined heat transmission after deleting tapered turbulators using various turbulators and funnel-shaped points of 50, 100, 150, and 200, finding that intensity move rate and grating coefficients increased [36]. Further analysis indicated that all increased cases had greater Nusselt number quality than the simple cylinder case, with 115.9% for 4.2 and 97% for 6.4 [37]. Turbulators increase choppiness power and reduce the heated limit layer thickness, increasing convection heat flow.

Others used COMSOL Multi-material science to accomplish CFD reproduction to investigate heat move improvement in round tubes with and without embeds for laminar stream from Re 1600 to 2400. With a continuous intensity motion of 32.087 KW/h, a non-isothermal stream model with water and copper round pipes was studied. The heat-transporting flow's dynamic behavior was explained using the non-isothermal flow governing equation and continuity equation [38]. Using four, six, and eight supplements on an 800-mm line, the highest yield temperature was 319.28 K for four additions. The cylinder without addition had a temperature of 307.85 K.

Additionally, adding supplements can promote heat movement. However, supplement spacing should be addressed. A recent study used mathematical methods to analyze the constant two-layered development of a thick liquid in a conduit under asymptotic limit circumstances. Many essayists have studied this stream. The Jeffery-Hamel (JH) stream's unsteadiness and bifurcation are explored while the channel transition is continually pushed [39]. Another study examined the solidity of going through a deviating pipe. It inferred speed profiles at edge shakiness using non-equal examination for small spots under four degrees [40]. A recent study cautiously examined the stream's speed profile and associated concerns across wandering channels and concluded that the arrangement could have been better [41].

Another investigation examined heat move intensifiers, surface unpleasantness, pierced confusion, and curved tape contained in tubes, showing that intensity transmission speeds up when an area alters [42]. Another study examined the spatially creating worldwide direct solidness investigation issue to show that unsettling influence modes are not wave-like irritations expected by neighborhood equal or feebly non-equal examinations and questioned the relationship between primary Reynolds number and vertex point. A turn-around stream with a high stormy stream may increase cylinder wall convection by increasing the crucial Reynolds number, decreasing the cross-segment stream area, and increasing the mean speed and temperature slope[43]. Recent research used shorter empty cone embeds to analyze heat transmission and friction in cylinders [44]. Roslim et al., [45] focused on V-spout turbulators' effects on cylinder heat transport and stream grating. They also tested how a funnel-shaped spout and snail entrance affected heat transport and grating in a uniform-intensity motion cylinder. Using both enhancement devices increased heat flow significantly. A parametric study of the laminar stream and intensity move qualities of curls formed from different cross-sectional area tubes were used to assess the mathematical influence on heat move execution [46]. Another ANSYS model is acquainted with a pattern of expanded heat moving with the supplement on the intensity exchanger in a twin line heat exchanger of width 0.015 m and length 2.5 m with variable turned type embed. Heat movement increased as the Reynolds number changed. Addiction's effect on heat move upgrade depends on the supplement and stream Re, which are directly measured using tapered rings as turbulators over a test tube. In the testing, funnel-shaped rings with three different measurement proportions of ring to width (d/D = 0.5, 0.6, 0.7) were used, and each proportion was organized in three different ways: concurrent, wandering, and veering joining, through which cold air at room temperature was conveyed [47].

This study aims to experimentally investigate heat transfer enhancement in a turbulent flow within a tube with an annular cross-section, focusing on the efficiency and practicality of a non-rotating, purely swirl-based flow design. The primary objective is to quantify the heat transfer improvement and determine the representative Nusselt number correlation, Nu=f(Re)Nu = f (Re)Nu=f(Re), to analyze the relationship between Reynolds and Nusselt numbers in this set-up.

This work's innovative contribution lies in the use of specially designed mounts with tangential flow inlets positioned upstream of the array to generate swirl flow without moving parts, such as rotating cylinders. This design choice not only simplifies construction and maintenance but also minimizes pressure drops commonly associated with vane-driven methods while enabling a straightforward sealing mechanism due to the tangential inlet. However, a noted limitation is the natural decrease in transport coefficients along the flow path, leading to reduced heat transfer efficiency as the flow progresses.

This study is important because it provides a practical and efficient alternative to traditional rotating devices, offering a lower-cost, lower-maintenance solution with significant industrial application potential. Statistical analysis and uncertainty evaluation will validate the heat transfer correlation and ensure the reliability of the results, underscoring this design's potential for enhancing heat transfer in engineering applications.

2. Experimental set-up

A sketch of the experimental set-up is shown in Figure 1. It is a system consisting of (in) the flow base, (ii) the concentric cylinder arrangement, and (iii) a suction fan. The design of the concentric cylinders and bases of the loops was such that the ratio of the thickness of the ring of the former (Rex. − Rin.) to the diameter of the loops ($D\beta$) was 1:1. Thus, "pure swirl flow" flow conditions are ensured [48]. The flow stands were located upstream of the array while the suction fan was downstream, capable of providing velocities up to 2 m/s at the array exit.

2.1. Flow Bases

Figure 2 shows that five flow bases were used: one axial and four eddy flow bases. The spindle bases (also referred to as loop bases in the text) were designed with four symmetrically arranged loops around their circumference, with an inclination (ϕ) relative to their cross-section. All bases were printed using a 3D printer and made from material resistant to thermal loads up to 150°C. They were engineered to fit securely with the cylinder system, with a small hole at the base allowing for the passage of thermocouples placed in the inner cylinder. The appropriate base creates the flow swirl, which introduces a tangential stream of air and cools the heated inner cylinder.

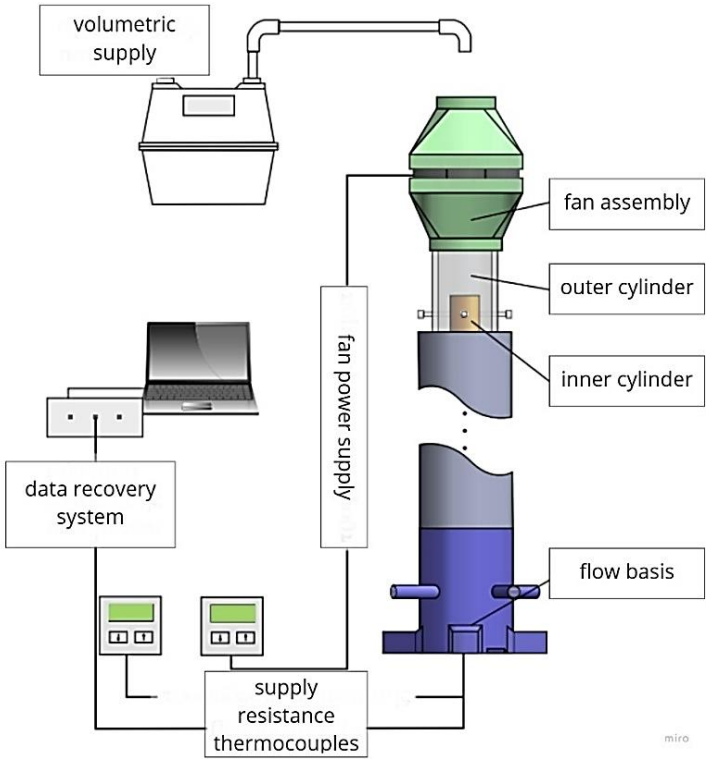

Figure 1. Sketch of experimental layout.

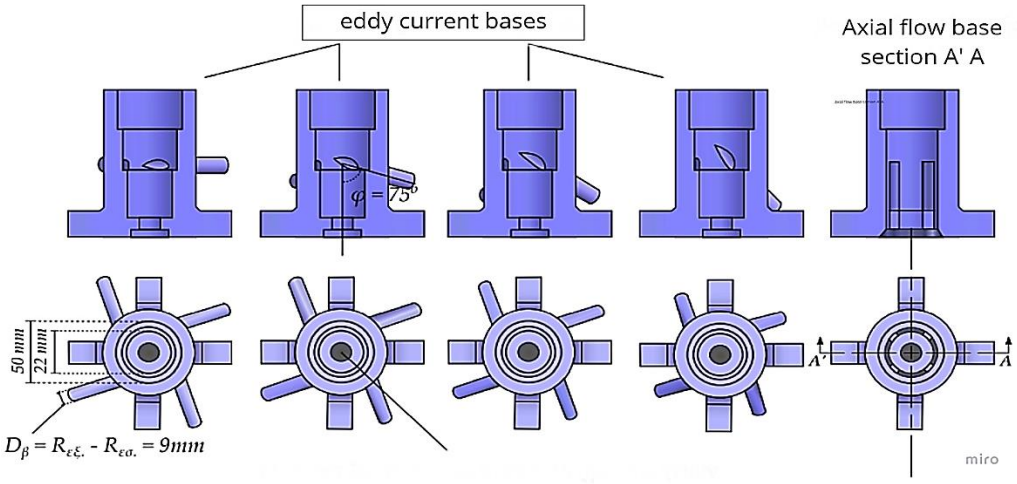

Figure 2. Flow bases.

 © 2025 Jordan Journal of Mechanical and Industrial Engineering. All rights reserved - Volume 19, Number 1 (ISSN 1995-6665)

2.2. Arrangement of Concentric Cylinders

The central part of the installation consists of two concentric cylinders, the inner (or resistance) and outer, between which the fluid flows.

2.2.1. Outer cylinder

The outer cylinder was a 40-mm inner diameter Plexiglass tube with a thickness of 5 mm and a length of 895 mm. The material was chosen to facilitate its further processing, in case it was needed, and its mechanical properties would contribute to the smooth conduct of the experiments—the material has a low coefficient of thermal conductivity and is transparent.Reflective surface material was wrapped around the outer cylinder to limit heat loss due to radiation from the inner to the outer cylinder. Another layer of insulation material was also added to reduce conduction losses.Finally, at the top of the outer cylinder, three M14 screws were placed to ensure its eccentricity with the inner cylinder and to reduce, as much as possible, the spatial errors.

2.2.2. Inner cylinder

Upstream of the system, a 22 mm diameter, 1 mm thick, and 900 mm long pipe was used, with one outlet covered to create the inner cylinder. Ceramic material, resistant to thermal loads, was placed inside the tube, and a resistance wire was uniformly wound around it in suitably formed grooves to achieve as uniform heating as possible. During the placement of the resistance wire, exceptional care was taken to avoid wrapping it to avoid short-circuiting it.

The resistance was supplied by a constant MERSAN-type voltage source, nominally 50 V. Since the voltage governing the cable must not be transmitted to the copper tube, Mica insulating tape, an electrically good insulator, and thermally conductive material, was used. The tape's placement overlapped the gap between grooves and coiled wire precisely and was as close as possible to the copper tube.

K-type thermocouples were used and placed in a uniform pattern along its inner surface with thermally conductive glue to determine the temperature along the surface of the copper tube. Because the thermocouples were placed inside the tube to not obstruct the flow field, they were sealed at the lower end of the resistance with silicone - a thermally conductive material but an electrically insulating one. At the bottom of the resistor, a suitable base was placed to be connected to the PTFE flux bases, which had a low heat transfer coefficient and resistance to high thermal loads.

2.2.3. Suction Fan

A Corsair Ice SP120 suction fan, rated at 24 V, was mounted on top of the array. To control the flow, the fan was connected to an EZ GP-4303D DC power supply, rated at 24 V. A particular case was created to connect with the volumetric flow meter to implement the fan with the array of concentric cylinders. This case was made of the same material as the flux bases, and its dimensional tolerance did not exceed, according to the manufacturer, at least 0.2 mm.

2.3. Instrumentation and data retrieval

Temperature, time, and voltage-current measurements were taken to investigate the heat transfer enhancement in the inner cylinder experimentally. The first ones were made using K-type thermocouples, time with a combination of a hand timer and flow meter, and voltage-current with a precision multimeter. Temperature measurements were recorded on a computer, while the rest were taken manually, analyzing the experimental uncertainty and the calculated quantities.

2.3.1. Type K Thermocouples

K-type thermocouples were used for temperature measurements. They were welded in the laboratory shortly before placement in the inner cylinder. There were eleven in total: nine measured local temperatures along the resistor, one downstream of the array for fluid inlet temperature, and one upstream for outlet temperature.

A KEITHLEY 2700-type multimeter was used to record the temperature and on-and-off resistance continuously. Unfortunately, this data could not be stored continuously due to the "deification" of the multimeter-computer software. However, it has been successfully used to control temperatures until they continuously converge to a constant value.

Due to their relatively simple use, thermocouples are the most common temperature measurement method. However, measurements can be (and usually are) significantly affected by convective heat loss and their soldering process. So, measurements tend to overestimate these valid values due to the effects of inertia and energy losses [49]. In the present work, no attempt was made to address these errors.

2.3.2. Natural Gas Meter

The natural gas meter is connected to the outlet of the fan assembly. It was used with a timer, which recorded the time required to pass 0.1 m3 of air in each experiment. All air supplies for each flow arrangement came from the suction fan, the speed of which was regulated using a direct current source. Due to age, a "relative calibration" was conducted with a hot filament to estimate its validity.

2.4. lows and Measurement Methodology

Having assembled the entire device, in the first stage, the operating conditions of the experiments and the methodology for the heat transfer evaluation of the spinning bases were defined. It was decided that in each experimental set-up, data would be obtained for four Reynolds numbers: 1100, 1400, 1700, and 2000 - a range that ensures laminar flow conditions for the set-up in question [50]. All quantities were time-invariant, such as permanent flow conditions prevailed. Therefore, there was continuous control of the thermocouples' readings until their values converged to a fixed value. Finally, in order to be able to compare heat transfer between devices, the electrical supply of the inner cylinder was the same for all experiments [51], with a current of 0.63 A and a voltage of 29.5 V, which gives the supplied electrical power of resistance $Qres.$ = 18.85 W. Experiments were conducted with all possible combinations of numbers (α) and slope

(ϕ) of loops for four Reynolds numbers. Also, four more experiments were conducted for the same Reynolds range using the axial flow set-up to have reference values for the heat transfer enhancement. In total, there were 68 experiments.

The experiments took place for two months, in October and November 2019. For consistency reasons, they started in the morning hours. They ended early in the afternoon of the same day to reduce the contribution of the external temperature factor, which increased noticeably at noon. Before starting the day's experiments, each time, the readings of the thermocouples along the inner cylinder were meticulously observed. These should always have an increasing value, reading them upstream of the cylinder due to natural air circulation.

Particular attention was paid to placing data acquisition devices and measuring systems to avoid possible movements and unnecessary disassembly during the experiments. Errors related to the incomplete binding of the cylinders may create leaks and, therefore, different flow conditions compared to those of the rest. In addition, any inadequacy in the alignment of the inner and outer cylinders can induce undesired changes in the flow field, leading to incorrect measurements. No attempt was made to assess the uncertainty associated with misalignment (spatial error). During the experiments, it was accepted, by convention, that the tolerances between the attached parts and their alignment were controlled quite effectively and that any uncertainties attributed to poor connection were negligible.

2.5. Calculations and uncertainty analysis

This section details the analytical methodology used for the thermodynamic investigation of concentric cylinder flow configurations, including spinning and axial arrangements. It covers (i) the data analysis and underlying assumptions, (ii) a thorough uncertainty analysis of measured values and their contribution to the results, and (iii) the relevant uncertainties along with the analytical results for the operational ranges studied. Uncertainty analysis is typically summarized in experimental studies [52], [53], reflecting the rigorous experimental set-up and the significant effort invested in code implementation, calculations, and literature review.

2.5.1. Reynolds Number Estimation

Sequel to Wang et al.,[54] andBelazreget al., [55], the Reynolds number helps determine whether a flow is laminar or turbulent. Laminar flow occurs at low Reynolds numbers (typically less than 2000), where the fluid flows in smooth, orderly layers. In agreement with Wang et al., [56], turbulent flow occurs at high Reynolds numbers (typically greater than 4000), where the flow is chaotic and mixed. The Reynolds number of each flow can be determined by calculating the flow. This dimensionless number equals the ratio of inertial and viscous forces and is used to determine the flow type:

$$D_h = \frac{\frac{4\pi\left(D_{\varepsilon\xi}^2 - D_{\varepsilon\sigma}^2\right)}{4}}{\pi\left(D_{\varepsilon\xi} + D_{\varepsilon\sigma}\right)} = D_{\varepsilon\xi} - D_{\varepsilon\sigma} \quad (1)$$

and the mean flow velocity,

$$\overline{U} = \frac{\dot{V}}{A_{ann}} \quad (2)$$

$$A_{ann} = \frac{\pi\left(D_{\varepsilon\xi}^2 - D_{\varepsilon\sigma}^2\right)}{4} \quad (3)$$

The Reynolds number can be obtained:

$$R_e = \frac{\rho \overline{U} D_h}{\mu} = \frac{4\rho\dot{V}}{\pi\mu\left(D_{\varepsilon\xi} + D_{\varepsilon\sigma}\right)} \quad (4)$$

2.5.2. Nusselt Number Estimation

The most common expression for determining the efficiency of heat transfer enhancement through forced flow is the dimensionless Nusselt number (Nu). This number expresses the heat transfer enhancement due to convection compared to conduction. It is usually a function of the geometrical characteristics of the system (x, L) and the Reynolds and Prandtl numbers:

$$N_{u_x} = f(x, R_{e_x}, P_r) \quad (5)$$

which for the assumption P_r = 1 becomes:

$$N_{u_x} = f(x, R_{e_x}) \quad (6)$$

In the present work, a representative Nusselt number for each arrangement is derived, with the Reynolds flow condition ranging from 1100 to 2000. This process is conducted in stages: (i) the local Nusselt numbers are calculated at the locations of the thermocouples for each array, (ii) the average Nusselt number is determined through statistical analysis of the individual local Nusselt numbers, and (iii) a forced regression is performed to establish a correlation function, from which the representative Nusselt number is estimated using a numerical integration method:

2.5.2.1. Local Nusselt:

The local Nusselt number is expressed as:

$$N_{u_x} = \frac{h_x D_h}{k_{\alpha\grave{\varepsilon}\rho\alpha}} = \frac{h_x\left(D_{\varepsilon\xi} - D_{\varepsilon\sigma}\right)}{k_{\alpha\grave{\varepsilon}\rho\alpha}} \quad (7)$$

Where hx the local convection coefficient, Dh the hydraulic diameter of the device, and $k$air the thermal conductivity of the air. Applying an energy balance at an infinitesimal distance from the surface of the inner cylinder, the local convection coefficient, in turn, is given by:

$$h_x = \frac{\dot{q}_{conv}}{T_{\alpha\nu\tau.,x} - T_{\alpha\grave{\varepsilon}\rho\alpha,x}} = \frac{\dot{Q}_{res}}{A_{heated}\left(T_{\alpha\nu\tau.,x} - T_{\alpha\grave{\varepsilon}\rho\alpha,x}\right)} = \frac{V_{\alpha\nu\tau.} A_{\alpha\nu\tau.}}{\frac{\pi D_{\varepsilon\sigma} L}{0.9}\left(T_{\alpha\nu\tau.,x} - T_{\alpha\grave{\varepsilon}\rho\alpha,x}\right)} \quad (8)$$

As in the case of thermocouples, Nux are governed by different uncertainties, so each calculation should be weighted differently according to its error. So, to combine each Nux into a total value Nu, the weighted average is used [39], [57]:

$$\overline{N_u} = \frac{\sum_{x=1}^{9} w_x N_{u_x}}{\sum_{x=1}^{9} w_x} \quad (9)$$

In calculating the representative power value ($Wavg$), the average Nusselt numbers Nu for four Reynolds values have been used. So, force regression can now be applied to derive a correlation relation for flow conditions 1100 to 2000 Reynolds.

2.6. Uncertainty analysis of individual measurements

In the experiments conducted, their execution time was approximately one and a half hours to ensure steady flow boundary conditions, which makes the replication of the experiments to find the repeatability of the measurements inauspicious in terms of time. Therefore, Single-Sample Uncertainty Analysis (also known as Single-Sample Uncertainty Analysis) was used [58]. Its philosophy is based on collecting data for a representative operating time before the start of experimental procedures. These data are analyzed, and conclusions about the system's behaviors are drawn. In general, this is a time-consuming but necessary (for reasons of experimental consistency) process, which includes the determination of (I) system error (zero-order error), (ii) errors due to various variables governing system operation (1st-order and higher-order errors) and (iii) error including the above as well as instrument calibration error (also known as *N*-order error). According to Moffat [59], the whole process should at least include the effects found in systematic and first-order errors. Given the available resources and time, the procedure followed was as follows:

1. The sensitivity error of the meter, $\delta Xsens$, was determined or obtained from relevant literature.
2. For each gauge, the zero-order error, $\delta X0$, was determined by taking 31 measurements5 while the experimental set-up was at rest, with conditions as stable as possible. For these data, the standard deviation was calculated from:

$$\sigma_x=\left\{\frac{1}{n-1}\sum_{i=1}^{n}(X_i-\bar{X})^2\right\}^{1/2} \quad (10)$$

$$\bar{X}=\frac{1}{n}\sum_{i=1}^{31}X_i \quad (11)$$

A typical uncertainty analysis aims to express the total uncertainty of a calculated variable F in the same confidence interval as the corresponding errors of the individual components of xi. For this purpose, the method of linear propagation of the error was used, which is based on the expansion of the Taylor series while maintaining the first-order differentials6. This approach, also known as Root-Sum-Squared or RSS, can calculate the total error fairly, as shown by Kline and McClintock[60].

3. Result and Discussion

The results extracted from the analytical operations of the computational routine in MATLAB® are presented (see Algorithm C′.8). Specifically: (i) the results of temperature homogeneity are shown, (ii) the regression models, along with the representative Nusselt and power values, are provided, and (iii) the improvement indices of the loop arrangements are detailed.

3.1. General Context

As of now, the gas turbine area depends on severe legitimate guidelines regarding poison emanations and decreased fuel utilization. To meet these necessities, avionics motors and modern gas turbines should work on their warm effectiveness. A fly motor comprises three sections: a blower, an ignition chamber, and a turbine. The blower increases gaseous tension, fuel is taken care of to the burning chamber, lighted, and a high-temperature stream is delivered. This high-pressure, high-temperature gas grows in the turbine, producing shaft work, raising the strain proportion across the turbine, and expanding the ignition temperature.

As a result, increasing the turbine's entry temperature can improve its thermal efficiency. Recently, the turbine inlet temperature has risen significantly above the melting point of the turbine blade material. Due to high thermal loads, the blades in the early turbine stages are equipped with an internal air-cooling system, as shown in Figure 3 (a cross-section of a turbine blade). Here, an interior serpentine cooling duct with ribs is depicted. Additionally, film cooling holes create an air film on the blade's exterior surface, protecting the material from hot gases. The cooling air for the blade cooling system is drawn from an upstream compressor stage, resulting in an air loss for combustion, which impacts the entire engine. Thus, a feasible cooling solution would require less cooling air from the compressor stage, allowing more air to support combustion and engine operation, thereby increasing overall efficiency.

The turbine's sharp edge driving edges are presented to the most noteworthy temperatures during the primary turbine stages, requiring the best inner air-cooling framework. For this reason, A twirl tube, likewise portrayed in the cross-part of the turbine edge in Figure 3, can be an extremely compelling cooling gadget. A whirl tube comprises at least one digressive channel stream that makes an exceptionally 3D twirling stream, as demonstrated in red in the primary edge of the edge on the left half of Figure 3. This whirling stream is recognized by high speeds close to the wall and expanded disturbance in the cylinder, increasing convective intensity multiple times when contrasted with a hub untwirled tube stream.

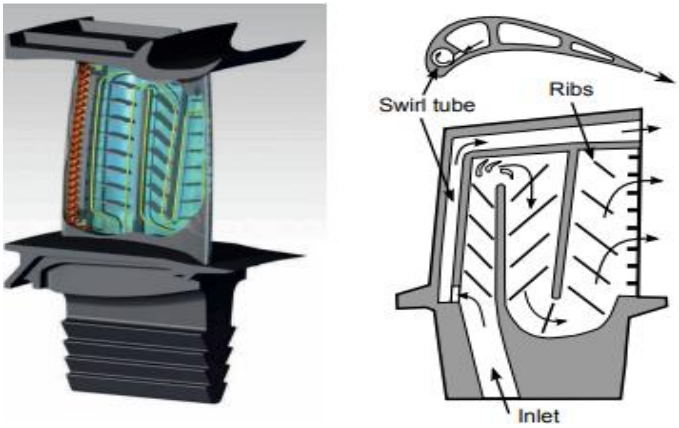

Figure 3. 3D turbine blade model and cross-section with leading-edge swirl tube [61]

3.2. Temperature Homogeneity

The measurements taken for each arrangement when steady flow conditions prevailed are shown in Appendix E′. It is not easy to draw any conclusion in such a form. Therefore, temperature profiles of the inner cylinders were created, and a related table was created where the weighted average values and their standard deviations were listed.

The temperatures along the duct at which the system equilibrated are shown in Figure 4 for axial flow arrangement and Figure 5 for loop arrangements. For the case of the axial flow (4 pairs of values in total), the statistical data are placed in the relevant figure. In comparison, those of the swirling flows (64 pairs of values) are reported in Table 1 to avoid overloading the relevant shape. It should be noted that the temperature profiles carry the value of the measured point temperature from each thermocouple, which, by convention, considering that it represents the relevant subsystem of the device, is taken as its representative value. So, the temperature profiles result from this generalization and should not, under any circumstances, be considered to have distinct accuracy.

Observing the temperature profiles, it has been concluded that in the case of the 90-degree loop arrangements, there is an inversion of the temperature profile of the inner cylinder. In all arrangements, including axial ones, the most significant cooling occurs upstream of the arrangement and then decreases. In contrast, in those with 90-degree loops, it occurs downstream because the fluid is injected perpendicular to the axis of symmetry of the annular tube, resulting in zero axial component (z) of the momentum [62]. There is a condensation of streamlines towards the outer cylinder. It is also indicative of the mistaken assumption of zero spatial error. Indeed, even if the lines acquire a zero axial momentum component, they should cool the resistance at the point of resistance, which is not the case.

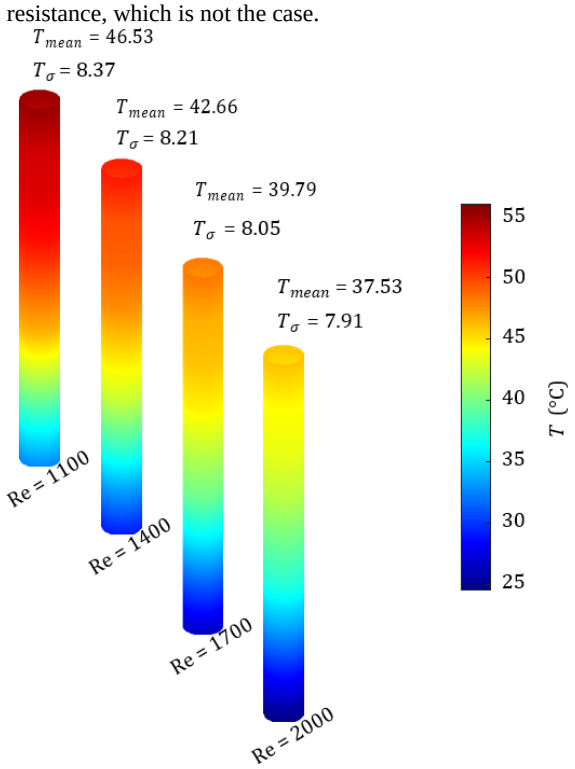

Figure 4. Temperature distribution along resistance for axial flow devices.

Table 1. Mean temperatures and standard deviations (°C) of swirling flow arrangements.

	$Re \simeq 1100$				$Re \simeq 1400$				$Re \simeq 1700$				$Re \simeq 2000$			
	$\alpha = 1$	$\alpha = 2$	$\alpha = 3$	$\alpha = 4$	$\alpha = 1$	$\alpha = 2$	$\alpha = 3$	$\alpha = 4$	$\alpha = 1$	$\alpha = 2$	$\alpha = 3$	$\alpha = 4$	$\alpha = 1$	$\alpha = 2$	$\alpha = 3$	$\alpha = 4$
Average layout price																
$\phi = 45°$																
τ_{mean}	45.46	46.77	47.55	48.19	42.88	44.33	45.46	45.92	40.91	42.45	43.84	44.17	39.34	40.95	42.53	42.75
$\phi = 60°$																
τ_{mean}	47.15	45.26	45.40	46.42	44.50	42.55	42.88	43.61	42.46	40.49	41.09	41.48	40.84	38.84	39.46	39.78
$\phi = 75°$																
τ_{mean}	49.92	46.02	45.63	46.48	44.06	42.84	42.77	44.09	41.88	40.43	40.60	42.26	40.15	38.52	38.87	40.79
$\phi = 90°$																
τ_{mean}	47.64	47.68	46.59	47.09	44.64	44.93	43.57	44.03	42.36	42.84	41.28	41.71	40.54	41.16	39.46	39.87
Standard deviation																
$\phi = 45°$																
$\tau_{\sigma,mean}$	5.85	5.55	5.85	5.92	5.42	5.18	5.33	5.43	5.10	4.90	4.93	5.06	4.84	4.68	4.62	4.76
$\phi = 60°$																
$\tau_{\sigma,mean}$	6.10	6.04	5.87	5.37	5.68	5.59	5.37	4.84	5.37	5.26	5.05	4.44	5.12	4.99	4.73	4.13
$\phi = 75°$																
$\tau_{\sigma,mean}$	6.39	6.11	5.80	5.61	6.02	5.71	5.31	5.11	5.74	5.41	4.94	4.74	5.52	5.18	4.66	4.44
$\phi = 90°$																
$\tau_{\sigma,mean}$	6.37	5.89	5.68	5.38	5.92	5.37	5.18	4.87	5.60	4.99	4.80	4.50	5.34	4.69	4.51	4.21

 © 2025 Jordan Journal of Mechanical and Industrial Engineering. All rights reserved

Table 1 summarizes the above data and reduces them to relative differences from the mean axial flow temperature. The abbreviations SMT and SD are Relative Mean and Confidence Interval, respectively.

The loop arrangements show less dispersion in the temperature measurements than the axial flow (8.14 °C). The maximum standard deviation is presented in the 75-degree and one-loop arrangement (5.91 °C), while the minimum is in the 90-degree and four-loop arrangement (4.73 °C). It is observed that the inner cylinder is cooled more unevenly for arrangements of one and three loops, in contrast to those of two and four loops, which indicates the symmetry of fluid injection concerning the vertical axis of the annulus, which the latter presents.

Table 2 Relative mean value and standard deviation of temperatures (in °C) for each experimental arrangement of loops as a function of the mean value of axial flow. Where ϕ and α the slope and number of loops, respectively.

3.3. Interference models and average values of power and Nusselt numbers

Table 3 has the parameters and uncertainties of the interference models for the correlations Nu = f (Re) and W = f (V–). It has been observed that the Pearson correlation coefficient (the term $r2$, also known as the coefficient of determination) [42] approached unity in all cases, which indicates the appropriateness of the interference models, at least as an initial estimate. Relationship Nu = f (Re) confirms the empirical relationship derived from the literature.

Having these data and applying relations 4.16 and 4.5, the representative Nusselt (Table 3) and the representative power values were found. The Nusselt-Reynolds number correlation plots and those of Power-output follow the annotations.

Table 2. Relative mean value and standard deviation of temperatures (in °C) for each experimental arrangement of loops as a function of the mean value of axial flow. Where ϕ and α the slope and number of loops, respectively

Layout ($\phi - \alpha$)	ΣMT	64% ΔE
45 – 1	0.52	(−4.78 με +5.82)
45 – 2	2.00	(−3.08 με +7.08)
45 – 3	3.22	(−1.97 με +8.40)
45 – 4	3.63	(−1.66 με +8.93)
60 – 1	2.11	(−3.46 με +7.68)
60 – 2	0.16	(−5.32 με +5.63)
60 – 3	0.58	(−4.68 με +5.83)
60 – 4	1.19	(−3.50 με +5.89)
75 – 1	1.63	(−4.29 με +7.54)
75 – 2	0.33	(−5.28 με +5.93)
75 – 3	0.34	(−4.84 με +5.52)
75 – 4	1.78	(−3.20 με +6.75)
90 – 1	2.17	(−3.64 με +7.97)
90 – 2	2.53	(−2.71 με +7.76)
90 – 3	1.10	(−3.95 με +6.14)
90 – 4	1.55	(−3.19 με +6.29)
axial	0.00	(−8.14 με +8.14)

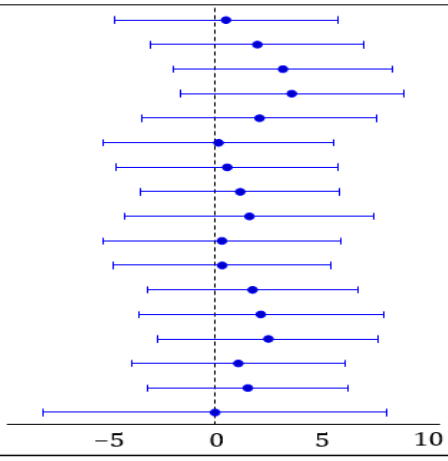

Table 3. Results of interference models

	$\overline{Nu} = aRe^b$					$W = aV^b$				
	a	σ_a	b	σ_b	r^2	$a \times 10^{-10}$	$\sigma_a \times 10^{-10}$	b	σ_b	r^2
$\phi = 45°$										
$\alpha = 1$	2.12	0.91	0.59	0.06	0.9765	1149.10	1702.43	3.73	0.22	0.9724
$\alpha = 2$	4.38	1.63	0.48	0.05	0.9951	0.68	1.00	2.83	0.22	0.9948
$\alpha = 3$	4.23	1.59	0.48	0.05	0.9989	0.08	0.14	2.60	0.26	0.9863
$\alpha = 4$	9.10	3.19	0.37	0.05	0.9913	0.01	0.01	2.16	0.26	0.9808
$\phi = 60°$										
$\alpha = 1$	5.21	1.98	0.45	0.05	0.9752	762.82	1083.21	3.67	0.21	0.9921
$\alpha = 2$	4.39	1.61	0.47	0.05	0.9863	3.62	5.27	3.04	0.22	0.9938
$\alpha = 3$	1.55	0.73	0.62	0.06	0.9812	70736.96	143638.32	4.47	0.30	0.9872
$\alpha = 4$	3.88	1.53	0.50	0.05	0.9990	0.09	0.17	2.63	0.27	0.9798
$\phi = 75°$										
$\alpha = 1$	3.02	1.28	0.53	0.06	0.9821	2694.81	4484.46	3.92	0.25	0.9934
$\alpha = 2$	1.85	0.77	0.61	0.06	0.9759	12.73	20.73	3.25	0.24	0.9648
$\alpha = 3$	2.18	0.91	0.58	0.06	0.9997	0.79	1.38	2.91	0.26	0.9920
$\alpha = 4$	2.35	0.99	0.56	0.06	0.9917	0.58	1.08	2.88	0.28	0.9960
$\phi = 90°$										
$\alpha = 1$	1.73	0.83	0.55	0.07	0.9998	14936.32	25208.21	4.14	0.25	0.9806
$\alpha = 2$	1.38	0.69	0.58	0.07	0.9982	76.27	142.51	3.51	0.28	0.9905
$\alpha = 3$	1.98	0.94	0.54	0.07	0.9789	2.15	3.99	3.05	0.28	0.9717
$\alpha = 4$	2.21	1.00	0.52	0.06	0.9756	0.22	0.41	2.75	0.27	0.9651
axial	1.23	0.62	0.64	0.07	0.9950	0.02	0.05	2.45	0.44	0.9974

3.4. Indicators of improvement

Using representative Nusselt numbers and power values and considering the amount of heat flow received by the air for each arrangement, it can now judge the improvement (where any) of the loop arrangements compared to that of axial flow.

As shown in Figure 5, most of the loop arrangements showed improved heat transfer. Only those with a 90-degree bronchial inclination did not show improvement. Among them, the maximum improvement was presented by the 45-degree and one-loop arrangement (24.32 ± 12.04 %), while the minimum value was presented by the 90-degree and one-loop arrangement (−24.45 ± 3.16 %).The uncertainties of the measurements ranged from 101.35 % of the indication for the 45-degree four-loop arrangement to 13.16 % for the 90-degree four-loop arrangement. Most of the prices could be more reliable. The errors of the fixed interference models (see Table 5) appear to bias the index calculations.

Table 4. Heat Transfer Improvement Index (HTII)

Bronchi angle	Number of loops							
	$\alpha = 1$		$\alpha = 2$		$\alpha = 3$		$\alpha = 4$	
	HTII	σ_{HTII}	HTII	σ_{HTII}	HTII	σ_{HTII}	HTII	σ_{HTII}
$\phi = 45°$	24.32	12.04	12.48	6.05	6.95	4.77	5.70	5.81
$\phi = 60°$	8.69	9.05	6.34	7.55	13.86	10.13	16.33	5.14
$\phi = 75°$	11.15	8.85	20.75	12.37	14.63	4.88	9.69	7.06
$\phi = 90°$	-24.95	3.16	-23.50	3.68	-18.96	7.21	-20.78	7.50

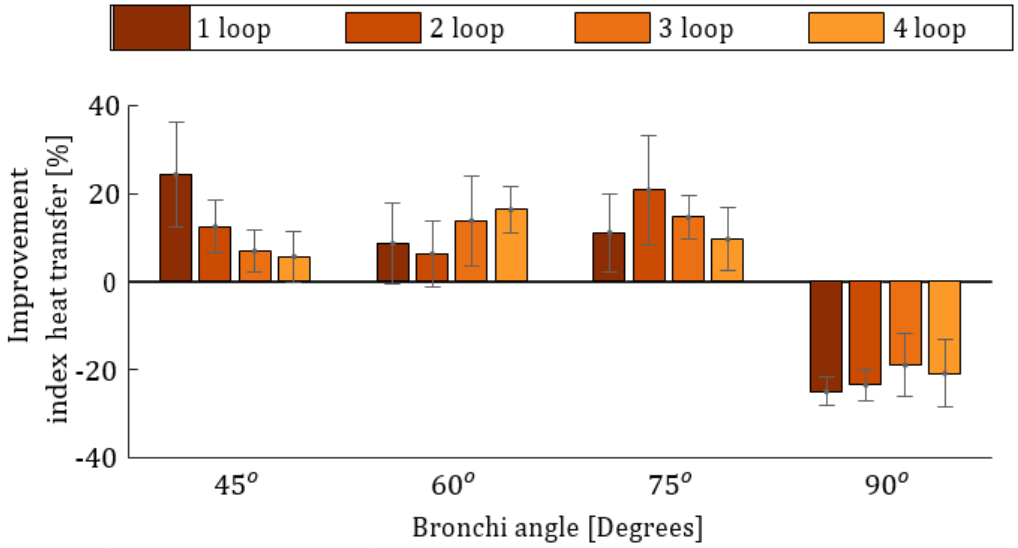

Figure 5. Heat transfer improvement index (HTII) for each angle and loop number combination compared to the simple axial flow case.

Table 5. Power Consumption Improvement Index (PII)

Bronchi angle	Number of loops							
	$\alpha = 1$		$\alpha = 2$		$\alpha = 3$		$\alpha = 4$	
	PII	σ_{PII}	PII	σ_{PII}	PII	σ_{PII}	PII	σ_{PII}
$\phi = 45°$	-1457.43	1540.37	-236.65	279.08	-92.32	370.21	-31.95	366.66
$\phi = 60°$	-1338.43	1458.93	-328.27	378.62	-612.90	470.01	-72.60	227.72
$\phi = 75°$	-904.64	476.40	-278.18	402.08	-133.91	147.19	-107.60	115.17
$\phi = 90°$	-1132.16	665.14	-334.46	197.27	-147.15	272.66	-82.05	317.21

 © 2025 Jordan Journal of Mechanical and Industrial Engineering. All rights reserved

As expected from the representative power values, the power required in the loop arrangements did not improve. However, the arrangement of 45 degrees and four loops showed the maximum improvement (−31.95 ± 366.66 %), while the arrangement of 45 degrees and one loop (−1457.43 ± 1540.37 %) showed the slightest improvement.Observing all the indices in Figure 6, for the considered loop arrangements that are increasing the number of loops, the power improvement index improves, which happens because to ensure the current flow conditions for a small number of loops, the injection of fluid is required from a smaller surface and therefore has more losses. The measurement errors were well above the acceptable limit. The maximum measurement error was presented by arranging 45 degrees and four loops (1180.64 % of the indication). In comparison, the minimum was 75 degrees and three loops (58.74 % of the indication).The payable Potential Improvement Index (PEI) is presented in Table 6.

The usable potential for all loop arrangements was negative. The electrical energy flow (i.e., the fan power consumption) was used more efficiently to increase the thermal energy flow to the air in the axial flow. However, the limitation to the loop arrangements is that the electric energy flow of the fan was better used for the 45-degree and one-loop system (−31.86 ± 19.01 %) and less favorable for the 45-degree and four-loop system (−88.93 ± 2.64 %).

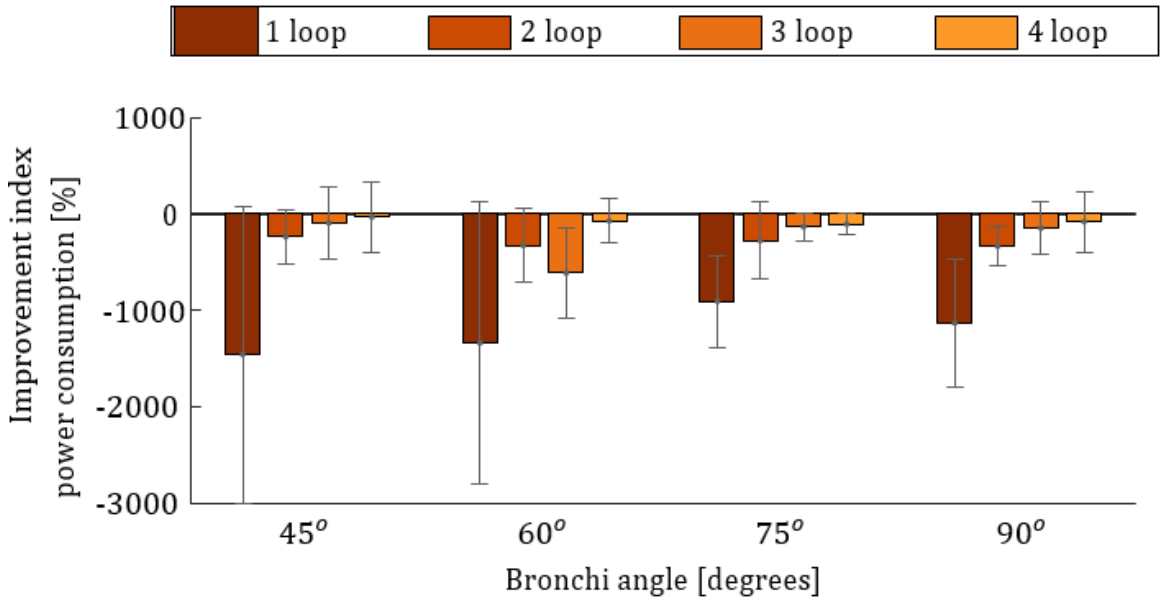

Figure 6. Power consumed improvement index (PII) for each combination of angle and loop numbers compared to the simple case of axial flow.

Table 6. Payable Potential Improvement Index (PEI)

Bronchi angle	Number of loops							
	$\alpha = 1$		$\alpha = 2$		$\alpha = 3$		$\alpha = 4$	
	PEI	σ_{PEI}	PEI	σ_{PEI}	PEI	σ_{PEI}	PEI	σ_{PEI}
$\phi = 45°$	-88.93	2.64	-64.69	8.97	-37.91	16.82	-31.86	19.01
$\phi = 60°$	-87.83	2.91	-71.22	7.25	-65.07	8.68	-44.46	14.98
$\phi = 75°$	-84.31	3.79	-69.00	7.89	-49.14	13.40	-33.73	17.84
$\phi = 90°$	-83.04	4.08	-62.40	9.57	-54.01	12.09	-42.10	15.62

3.5. Heat Transfer

As far as circumferentially arrived at the midpoint of Nusselt numbers, the intensity transmission information is given below. For a wholly created hub tube stream, the Nusselt numbers are standardized by the Nusselt number Nu0. The Dittus-Boelter connection is used here, given by Nu0 = 0.023 Re0.8P r0.3 [63], which is additionally noted in segment 2.1 for the Nusselt number relationships. The mean Reynolds number from every preliminary is used for standardization, as referenced in area 3.6. The intensity moves discoveries for the four Reynolds numbers (10,000 40,000), eight different whirl numbers (0.75 5.3), and three outlet calculations (straight, unrelated, and 180 twist outlet) are thought about.Figure 7 depicts a detailed overview of the local wall heat flow distribution. The numerical findings for the swirl number S = 5.3 and the Reynolds number Re = 10,000 are shown. The wall heat flow consistently reduces the tube's length. The spiral stripes surrounding the tube clearly show the effect of the helical vortex structure on the wall heat flow.

Figure 7 portrays the Nusselt numbers with mistake bars for the most significant twirl number S = 5.3 (a) and S = 2.95 (b) (b). The Nusselt number blunder bar is 13% in the channel zone and 8% in the power source locale. The standardized intensity moves values cross over for all Reynolds numbers tried, inferring that the spinning stream is compared to Re0.8, much the same as a pivotal cylinder stream with a considerable outcome since it permits the heat move information to be scaled. Due to the significant circumferential speed part in this area, the greatest Nusselt values close to the bay are multiple times higher than those for the pivotal cylinder stream. Indeed, even at S = 2.95, the intensity improvement is a variable of 5. Heat moving towards the cylinder outlet constantly diminishes as twirl and speed decline. At the power source, the Nusselt number is over twice as prominent for S = 5.3 and twice as high for S = 2.95 than for the pivotal stream. The critical reason for the expanded intensity moves in the twirl tubes is the circumferential speed with enormous angles close to the wall. The speed falls by a variable of three towards the wall, as shown in the speed dispersion in Figure 8, which relates to the Nusselt number diminishing in Figure 8 (a).

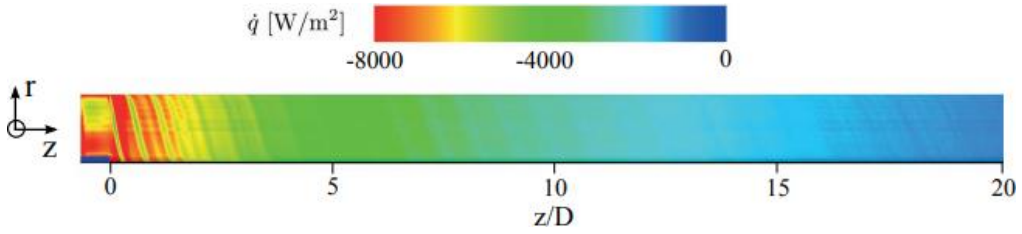

Figure 7. DES wall heat flux for S = 5.3 and Re = 10,000

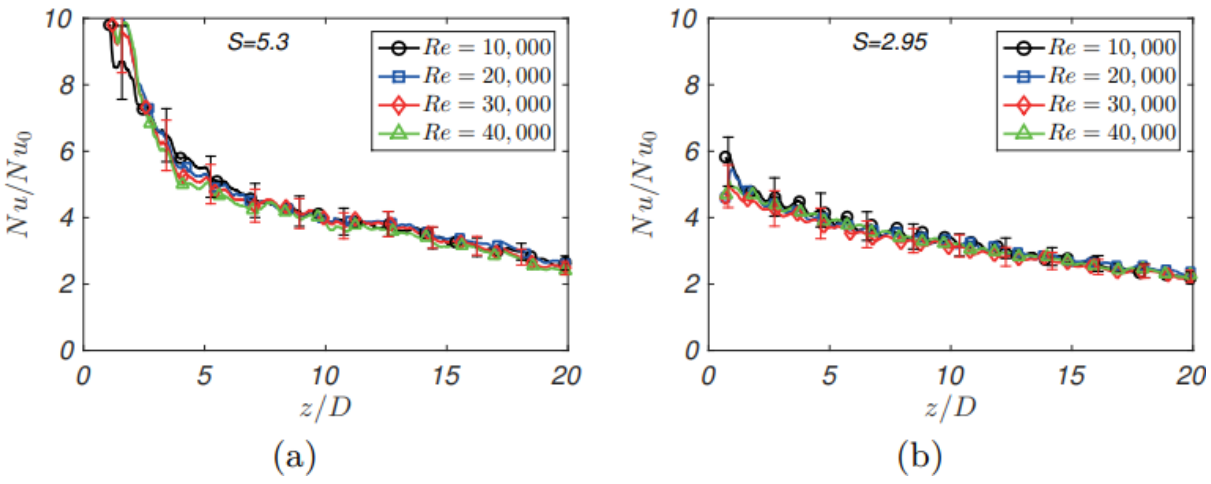

Figure 8. Experimental normalized Nusselt numbers for different Reynolds numbers. (a) S = 5.3, (b) S = 2.95

The twirl numbers examined shift from 5.3 to 0.75. The intensity transmission ascends with an expanded twirl number and, in this way, higher circumferential speed close to the wall. The Nusselt values for the dissected twirl numbers range from 3 to 10, close to the admission and reduction towards the cylinder outlet. The intensity move upgrade at the source for the most reduced twirl number S = 0.75 is around 1.2. So, all Nusselt numbers are higher across the whole cylinder than in a hub tube stream, exhibiting that spinning streams further develop heat transmission in tubes.Figure 8 (b) portrays the intensity move correlation for the three outlet calculations examined: straight, distracting, and 180 twist outlets. The Nusselt numbers for S = 5.3 and Re = 30,000 are plotted here. The intensity move bend is almost indistinguishable from Figure 8 (a), with a most extreme Nusselt number improvement of 10 close to the admission and a drop towards the cylinder outlet. The Nusselt numbers show practically little distinction between the three outlet shapes. Thus, the researched outlet redirection significantly affects upstream intensity transmission. Subsequently, the twirling stream in the tubes investigated here has a vigorous plan for different whirl qualities and outlet conditions, making it suitable for cooling high thermally stacked parts.

Regarding power consumption and functional potential, no improvement was shown in any of the arrangements to be expected, considering the nature of swirling flows. The maximum required power was 1457.43 % more than the axial, while the lowest applicable potential value reached 88.93 % of the axial. In the uncertainty analysis, the errors in the results of the initial calculations were within tolerable limits, less than 4.5 % of the readings. However, the local Nusselts presented uncertainties ranging from 5 % to 8 % of their index. In calculating the improvement indices, the uncertainties seemed to "escape," thus precipitating any substance the results had. Specifically, the errors of thermal improvement readings ranged from 13.16 % to 101.35 % of reading, power consumption improvement from 58.74 % to 1180.64 % of reading, and valuable potential from 2.9 % to 59.64 % of reading indication.

4. Conclusions

This study investigated heat transfer enhancement through fluid injection via loops to create circulating flow, using experimental methods. The work focused on two main aspects: (i) uncertainty analysis of core thermodynamic quantities, and (ii) assessing the influence of loop number (α) and inclination (ϕ) on heat transfer. Experiments were conducted in an annular duct under laminar flow conditions, with Reynolds numbers ranging from 1100 to 2000, examining temperature homogeneity, heat transfer improvement, power consumption, and functional potential.

Results indicate that swirling flows can improve heat transfer, with observed enhancements of up to 24.23%. Homogeneous cooling was better achieved with devices featuring an even number of loops, while configurations with 90-degree inclined loops showed a reduction in heat transmission by up to 24.45%. However, no improvement in power consumption or functional potential was observed, which aligns with the inherent energy demands of swirling flows. Maximum power requirements were 1457.43% higher than the axial configuration, while the minimum applicable potential reached 88.93% of axial values.

In uncertainty analysis, primary calculation errors remained within acceptable limits, below 4.5%, though local Nusselt values presented uncertainties of 5% to 8%. Improvement indices showed wider uncertainty ranges, with thermal improvement errors between 13.16% and 101.35%, power consumption improvement from 58.74% to 1180.64%, and functional potential from 2.9% to 59.64%. These findings support further exploration into fluid injection methods for enhanced heat transfer.

References

[1] J. Zhong, D. Wang, and C. Sun, “From sheared annular centrifugal Rayleigh–Bénard convection to radially heated Taylor–Couette flow: exploring the impact of buoyancy and shear on heat transfer and flow structure,” *J. Fluid Mech.*, vol. 972, p. A29, 2023.

[2] T. Rahman, “Advection-Enhanced Mass Transport from Neutrally Suspended Twisted Cuboid in Simple Shear Flow.” New Mexico State University, 2024.

[3] C. Strassel *et al.*, “Uniform impact on individual megakaryocytes is essential for efficient in vitro platelet production,” 2024.

[4] R. Jefferson-Loveday, G. Gennari, S. Pickering, and M. George, “Bubble dissolution in Taylor-Couette flow,” *J. Fluid Mech.*, 2024.

[5] S. Naz and T. Renganathan, “An exact asymptotic solution for a non-Newtonian fluid in a generalized Couette flow subject to an inclined magnetic field and a first-order chemical reaction,” *AIMS Math.*, vol. 9, no. 8, pp. 20245–20270, 2024.

[6] Y. He, Q. Hong, D. Zhang, and B. Kong, “Evaluation of Droplets Breakup Models of Emulsification Process in a Liquid–Liquid Taylor–Couette Flow,” *Ind. Eng. Chem. Res.*, vol. 63, no. 18, pp. 8401–8415, 2024.

[7] A. Ohsawa, A. Murata, and K. Iwamoto, “Through-flow effects on Nusselt number and torque coefficient in Taylor-Couette-Poiseuille flow investigated by large eddy simulation,” *J. Therm. Sci. Technol.*, vol. 11, no. 2, pp. JTST0031–JTST0031, 2016.

[8] S. L. Ghashim, “Experimental Study on Heat Dissipation in Metallic Foam Filled Heat Sink.,” *Jordan Journal of Mechanical and Industrial Engineering*, vol. 18, no. 3, 2024.

[9] M. Shareef, “MHD Flow Along a Vertical Plate with Heat and Mass Transfer under Ramped Plate Temperature.,” *Jordan Journal of Mechanical and Industrial Engineering*, vol. 17, no. 2, 2023.

[10] R. M. K. Ali and S. L. Ghashim, “Thermal performance analysis of heat transfer in pipe by using metal foam.,” *Jordan Journal of Mechanical and Industrial Engineering*, vol. 17, no. 2, 2023.

[11] Ł. J. Orman, “Enhanced Boiling Heat Transfer on Surfaces Covered with Microstructural Mesh Coatings.,” *Jordan Journal of Mechanical and Industrial Engineering*, vol. 13, no. 3, 2019.

[12] A. H. Haleem, N. S. Radhi, N. T. Jaber, and Z. Al-Khafaji, “Preparation and Exploration of Nano-Multi-Layers on 316l Stainless Steel for Surgical Tools,” *Jordan Journal of Mechanical and Industrial Engineering*, vol. 18, no. 2, pp. 339–350, 2024.

[13] A. K. AL-Migdady, A. M. Jawarneh, A. K. Ababneh, and H. N. Dalgamoni, “Numerical Investigation of the Cooling Performance of PCM-based Heat Sinks Integrated with Metal

Foam Insertion.," *Jordan Journal of Mechanical and Industrial Engineering*, vol. 15, no. 2, 2021.

[14] Y. Al-Abayechi, Y. Alaiwi, and Z. Al-Khafaji, "Exploration of key approaches to enhance evacuated tube solar collector efficiency," *J. Adv. Res. Numer. Heat Transf.*, vol. 19, no. 1, pp. 1–14, 2024.

[15] M. A. Sharaf-eldin *et al.*, "Modifying Walk-In Tunnels through Solar Energy , Fogging , and Evaporative Cooling to Mitigate Heat Stress on Tomato," 2023.

[16] D.-D. Dang, X.-T. Pham, P. Labbe, F. Torriano, J.-F. Morissette, and C. Hudon, "CFD analysis of turbulent convective heat transfer in a hydro-generator rotor-stator system," *Appl. Therm. Eng.*, vol. 130, pp. 17–28, 2018.

[17] A. Ben Nachouane, A. Abdelli, G. Friedrich, and S. Vivier, "Numerical approach for thermal analysis of heat transfer into a very narrow air gap of a totally enclosed permanent magnet integrated starter generator," in *2015 IEEE Energy Conversion Congress and Exposition (ECCE)*, IEEE, 2015, pp. 1749–1756.

[18] A. M. Jawarneh, M. Al-Widyan, and Z. Al-Mashhadani, "Experimental study on heat transfer augmentation in a double pipe heat exchanger utilizing jet vortex flow," *Heat Transf.*, vol. 52, no. 1, pp. 317–332, 2022, doi: 10.1002/htj.22696.

[19] A. M. Jawarneh, M. Al-Widyan, A. Al-Migdady, H. Tlilan, M. Tarawneh, and A. Ababneh, "Double vortex generators for increasing the separation efficiency of the air separator," *Int. J. Heat Technol.*, vol. 35, no. 3, pp. 529–538, 2017, doi: 10.18280/ijht.350309.

[20] A. M. Jawarneh, "Investigation of the flow characteristics in a sink-swirl flow within two disks," *Int. Rev. Mech. Eng. IREME*, vol. 7, 2013.

[21] A. M. Jawarneh, "Heat Transfer Enhancement in a Narrow Concentric Annulus in Decaying Swirl Flow," *Heat Transf. Res.*, vol. 42, no. 3, pp. 199–216, 2011, doi: 10.1615/heattransres.2011001197.

[22] R. K. Shah and A. L. London, *Laminar flow forced convection in ducts: a source book for compact heat exchanger analytical data*. Academic press, 2014.

[23] S. Kakac, Y. Yener, and A. Pramuanjaroenkij, *Convective heat transfer*. CRC press, 2013.

[24] A. C. Yunus, "Heat transfer: a practical approach," *MacGraw Hill, New York*, vol. 210, 2003.

[25] C. J. Roos, *Clean heat and power using biomass gasification for industrial and agricultural projects*. Northwest CHP Application Center Olympia, WA, USA, 2010.

[26] A. M. Jawarneh and G. H. Vatistas, "Reynolds Stress Model in the Prediction of Confined Turbulent Swirling Flows," *J. Fluids Eng.*, vol. 128, no. 6, pp. 1377–1382, 2006, doi: 10.1115/1.2354530.

[27] A. M. Jawarneh, G. H. Vatistas, and Y. Aboelkassem, "Experimental Investigation of the Pressure Drop in a Sink-Swirl Flow Within Two Disks," *J. Propuls. Power*, vol. 21, no. 4, pp. 759–760, 2005, doi: 10.2514/1.13026.

[28] F. Kreith and M. S. Bohn, "Principles of heat transfer, St," *Paul West Publ. Co.*, 1993.

[29] R. Razgaitis and J. P. Holman, "A survey of heat transfer in confined swirl flows," *Futur. energy Prod. Syst. Heat mass Transf. Process.*, vol. 2, pp. 831–866, 1976.

[30] T. H. Kuehn and R. J. Goldstein, "An experimental and theoretical study of natural convection in the annulus between horizontal concentric cylinders," *J. Fluid Mech.*, vol. 74, no. 4, pp. 695–719, 1976.

[31] A. M. Jawarneh, P. Sakaris, and G. H. Vatistas, "Experimental and analytical study of the pressure drop across a double-outlet vortex chamber," 2007.

[32] A. M. Jawarneh, G. H. Vatistas, and H. Hong, "On flow development in jet-driven vortex chambers," *J. Propuls. power*, vol. 21, no. 3, pp. 564–570, 2005.

[33] M. Yilmaz, S. Yapici, Ö. Çomakli, and O. N. Şara, "Energy correlation of heat transfer and enhancement efficiency in decaying swirl flow," *Heat mass Transf.*, vol. 38, no. 4, pp. 351–358, 2002.

[34] S. Hossain, U. K. Deb, and K. A. Rahman, "The enhancement of heat transfer in a circular tube with insert and without insert by using the finite element method," *Procedia Eng.*, vol. 105, pp. 81–88, 2015.

[35] I. E. Idelchik, M. O. Steinberg, and O. G. Martynenko, *Handbook of hydraulic resistance*, vol. 2. Hemisphere publishing corporation New York, 1986.

[36] H. Karakaya and A. Durmuş, "Heat transfer and exergy loss in conical spring turbulators," *Int. J. Heat Mass Transf.*, vol. 60, pp. 756–762, 2013.

[37] V. Kongkaitpaiboon, K. Nanan, and S. Eiamsa-Ard, "Experimental investigation of heat transfer and turbulent flow friction in a tube fitted with perforated conical-rings," *Int. Commun. Heat Mass Transf.*, vol. 37, no. 5, pp. 560–567, 2010.

[38] F. Kreith and D. Margolis, "Heat transfer and friction in turbulent vortex flow," *Appl. Sci. Res. Sect. A*, vol. 8, pp. 457–473, 1959.

[39] W. Liu, Z. Liu, and Z. Guo, "Physical quantity synergy in laminar flow field of convective heat transfer and analysis of heat transfer enhancement," *Chinese Sci. Bull.*, vol. 54, no. 19, pp. 3579–3586, 2009.

[40] W. Liu, Z. Liu, and L. Ma, "Application of a multi-field synergy principle in the performance evaluation of convective heat transfer enhancement in a tube," *Chinese Sci. Bull.*, vol. 57, pp. 1600–1607, 2012.

[41] R. M. Manglik and A. E. Bergles, "Fully developed laminar heat transfer in circular-segment ducts with uniform wall temperature," *Numer. Heat Transf. Part A Appl.*, vol. 26, no. 5, pp. 499–519, 1994.

[42] J.-A. Meng, X.-G. Liang, and Z.-X. Li, "Field synergy optimization and enhanced heat transfer by multi-longitudinal vortexes flow in tube," *Int. J. Heat Mass Transf.*, vol. 48, no. 16, pp. 3331–3337, 2005.

[43] M. Mirzaei and A. Sohankar, "Heat transfer augmentation in plate finned tube heat exchangers with vortex generators: a comparison of round and flat tubes," *Iran. J. Sci. Technol. Trans. Mech. Eng.*, vol. 37, no. M1, p. 39, 2013.

[44] A. A. Mohammed, B. A. Mohammed, and R. J. Muhee, "Heat Transfer Enhancement in a Tube Fitted with NozzleTurbulators, Perforated Nozzle-Turbulators with Different hole shap," *Eng. Technol. J.*, vol. 32, no. 10 Part (A) Engineering, 2014.

[45] M. K. Roslim, S. Hassan, and A. Tesfamichael, "Experimental investigation on heat transfer enhancement by using porous twisted plate as an insert in a fitted tube," *ARPN J. Eng. Appl. Sci.*, vol. 10, no. 21, pp. 10164–10168, 2015.

[46] G. Nagarajan and S. Ranganathan, "Heat transfer enhancement in double pipe heat exchanger with twisted type inserts in ANSYS fluent," *Int. J. Eng. Dev. Res.*, vol. 3, no. 2, 2015.

[47] F. Ribeiro, K. E. de Conde, E. C. Garcia, and I. P. Nascimento, "Heat transfer performance enhancement in compact heat exchangers by the use of turbulators in the inner side," *Appl. Therm. Eng.*, vol. 173, p. 115188, 2020.

[48] P. Promvonge and S. Eiamsa-Ard, "Heat transfer behaviors in a tube with combined conical-ring and twisted-tape insert," *Int. Commun. Heat Mass Transf.*, vol. 34, no. 7, pp. 849–859, 2007.

[49] F. Hasim, M. Yoshida, and H. Miyashita, "Compound heat transfer enhancement by a combination of a helically ribbed tube with twisted tape inserts," *J. Chem. Eng. Japan*, vol. 36, no. 9, pp. 1116–1122, 2003.

[50] A. Fan, J. Deng, J. Guo, and W. Liu, "A numerical study on thermo-hydraulic characteristics of turbulent flow in a

circular tube fitted with conical strip inserts," *Appl. Therm. Eng.*, vol. 31, no. 14–15, pp. 2819–2828, 2011.

[51] A. Savekar, D. Jangid, M. Gurjar, V. Patil, and C. Sewatkar, "Analysis of heat transfer in pipe with twisted tape inserts," *143*, 2015.

[52] C. BR, "Determination of principal characteristics of turbulent swirling flow along annuli," *Int J Heat Fluid Flow*, vol. 6, no. 1, pp. 31–41, 1985.

[53] E. G. Narezhnyy and A. V Sudarev, "Local heat transfer in air flowing in tubes with a turbulence promoter at the inlet," *İnt. J. Heat Mass Transf.*, vol. 3, pp. 62–66, 1971.

[54] F. Wang, I. L. Animasaun, Q. M. Al-Mdallal, S. Saranya, and T. Muhammad, "Dynamics through three-inlets of t-shaped ducts: Significance of inlet velocity on transient air and water experiencing cold fronts subject to turbulence," *Int. Commun. Heat Mass Transf.*, vol. 148, p. 107034, 2023.

[55] A. Belazreg *et al.*, "Insight into latent heat thermal energy storage: RT27 phase transition material conveying copper nanoparticles experiencing entropy generation with four distinct stepped fin surfaces," *Int. J. Thermofluids*, vol. 19, p. 100368, 2023.

[56] F. Z. Wang, I. L. Animasaun, T. Muhammad, and S. S. Okoya, "Recent advancements in fluid dynamics: drag reduction, lift generation, computational fluid dynamics, turbulence modelling, and multiphase flow," *Arab. J. Sci. Eng.*, pp. 1–13, 2024.

[57] A. A. Feiz, M. Ould-Rouis, and G. Lauriat, "Large eddy simulation of turbulent flow in a rotating pipe," *Int. J. heat fluid flow*, vol. 24, no. 3, pp. 412–420, 2003.

[58] P. Sivashanmugam and S. Suresh, "Experimental studies on heat transfer and friction factor characteristics of laminar flow through a circular tube fitted with regularly spaced helical screw-tape inserts," *Exp. Therm. Fluid Sci.*, vol. 31, no. 4, pp. 301–308, 2007.

[59] R. J. Moffat, "Describing the uncertainties in experimental results," *Exp. Therm. fluid Sci.*, vol. 1, no. 1, pp. 3–17, 1988.

[60] S. J. Kline, "The purposes of uncertainty analysis," 1985.

[61] A. Dewan, P. Mahanta, K. S. Raju, and P. S. Kumar, "Review of passive heat transfer augmentation techniques," *Proc. Inst. Mech. Eng. Part A J. Power Energy*, vol. 218, no. 7, pp. 509–527, 2004.

[62] W. R. Gambill and R. D. Bundy, "High-flux heat transfer characteristics of pure ethylene glycol in axial and swirl flow," *AIChE J.*, vol. 9, no. 1, pp. 55–59, 1963.

[63] P. Naphon, "Heat transfer and pressure drop in the horizontal double pipes with and without twisted tape insert," *Int. Commun. Heat Mass Transf.*, vol. 33, no. 2, pp. 166–175, 2006.